Fermi surface and magnetic properties of CeTe

M. Nakayama, N. Kimura, H. Aoki, and A. Ochiai*
Center for Low Temperature Science, Tohoku University, Sendai 980-8578, Japan

C. Terakura, T. Terashima, and S. Uji
National Research Institute for Metals, Tsukuba, Ibaraki 305-0047, Japan
(Received 11 November 2003; revised manuscript received 5 April 2004; published 26 August 2004)

We have grown high quality single crystals of the Kondo compound CeTe and its reference compounds LaX_c's with X_c=S, Se, Te, and measured the de Haas-van Alphen effect of these compounds and the magnetic properties of CeTe. The Fermi surface of each LaX_c is centered at the X points of the Brillouin zone and has a nearly ellipsoidal shape. The cyclotron effective masses are very close to the electron rest mass. On the other hand, CeTe has a rather complicated magnetic phase diagram which is different from that predicted by previous works. In the induced ferromagnetic phase of CeTe, the Fermi surface is found to be similar to that of LaTe but it splits into the majority and minority spin Fermi surface due to the exchange interaction between the $4f$ and conduction electrons. We have also observed strongly enhanced cyclotron effective masses in that phase. Interestingly, the mass enhancement of the minority spin surface differs with that of the majority spin surface by about a factor of 2.

DOI: 10.1103/PhysRevB.70.054421 PACS number(s): 75.30.Kz, 71.27.+a, 71.18.+y

I. INTRODUCTION

Rare-earth monochalcogenides (RX_c's with X_c=S, Se, Te) have been intensively studied because of various attractive properties and also because of the simple NaCl-type crystal structure. For example, SmS shows the pressure-induced metal-insulator transition, and TmSe shows the anomalous valence fluctuating state.[1,2] These interesting phenomena have been thought to originate from the interaction between the $4f$ and conduction electrons. Among them, Ce monochalcogenides (CeX_c's) are regarded as the most simple system because the Ce ion is in the trivalent state with one $4f$ electron. However, even in such simple CeX_c's the physical properties are still not well understood.

CeX_c's have been thought to be typical Kondo compounds that coexist with the magnetic order because the magnetic part of electrical resistivity clearly exhibits a logarithmic increase with decreasing temperature.[3] The cubic crystal field splits the lowest-lying J multiplet (J=5/2) into the Γ_7 doublet grand state and the Γ_8 quartet excited state.[5,6] At low temperatures, CeX_c's enter the type-II antiferromagnetic state which probably has the four-$\boldsymbol{k}$ structure.[7,8] We list some magnetic properties of these compounds together with the lattice constant in Table I. All the values for the magnetic properties are largest for CeS, and become smaller for CeSe. Those for CeTe are much smaller than those for CeS and CeSe. Particularly, that of the magnetic moment is considerably reduced from $0.71\mu_B$ which is expected for the Γ_7 doublet grand state.

It is well known for Ce compounds that application of pressure enhances both the Kondo effect and the magnetic Ruderman-Kittel-Kasuya-Yosida interaction. The chemical pressure increases by replacing the chalcogen element from Te to Se, and then to S, because the lattice constant decreases with the replacement. Since the Néel temperature (T_N) increases with increasing chemical pressure as noted from Table I, one may expect that the Kondo effect also increases and consequently the magnetic moment decreases. However, this is contrary to the experimental observation.

It has been also found by our angle-resolved photoemission spectroscopy (ARPES) measurements that CeTe has a peculiar electronic band structure compared with CeSe and CeS.[10] In CeTe as well as in CeS and CeSe a dispersionless band is observed well below the Fermi level (E_F) which is ascribed to the localized $4f$ states. However, only for CeTe a dispersive band is also observed close to the f band and in a very narrow region around the Γ point. Although this band mostly arises from the valence p band, we found that the hybridization between the $4f$ state and the valence p band plays a significant role for this band. From this fact and the observation that the electronic band structure systematically change in CeX_c's, we suspect that the intersite d-f hybridization through the valence p band probably plays an important role for the magnetic properties such as the small magnetic moment. Therefore, further extensive investigation on the electronic structure will certainly give important information to understand physical properties of CeTe. The de Haas-van

TABLE I. Lattice constant at room temperature (a), Néel temperature (T_N), crystal field splitting energy (Δ_{cry}), and magnetic moment in the ordered sate of CeX_c's.

	a(Å)	T_N(K)	Δ_{cry}(K)	Magnetic moment (μ_B)
CeS	5.7761[a]	8.4[b]	140[a]	0.57[a]
CeSe	5.992[c]	5.4[c]	116[a]	0.56[c]
CeTe	6.361[c]	2.2[c]	32[d]	0.30[e]

[a]Reference 5.
[b]Reference 6.
[c]Reference 7.
[d]Reference 9.
[e]Reference 4.

Alphen (dHvA) effect measurement is another powerful tool to investigate the electronic structure. Particularly, it is very useful to investigate the interaction between the $4f$ and conduction electrons as well as the Fermi surface topology. However, a long mean free path of the conduction electron is necessary for the detection of the dHvA signals. The sample qualities in preceding works are not enough to detect the dHvA signals. High quality single crystals that have good stoichiometry and high purity have been awaited.

In this paper, following the high quality single crystal growth of LaX_c's and CeTe, we will present the dHvA effect measurements of reference materials LaX_c's. Then, the measurements of the magnetization and dHvA effect for CeTe will be presented. We will show that the magnetic properties of CeTe are considerably sample dependent and its magnetic phase diagram obtained in this study is different from that predicted by previous works. Furthermore, we will show that the mass enhancement of the minority spin band differs from that of the majority spin band by a factor of 2.

II. SAMPLE PREPARATION AND EXPERIMENT

Single crystals of LaX_c's and CeTe were prepared by the following procedure. Starting materials are La or Ce with 4N purity (Ames laboratory) and S, Se, or Te with 6N purity. In the cases of LaS and LaSe, the starting materials were sealed in an evacuated silica tube and then the prereaction was carried out in a conventional electric furnace to avoid evaporation of the constituent elements at the next procedure. Then the prereacted powder was sealed in a tungsten crucible using an electron beam welder. In the case of LaTe and CeTe, the starting materials were directly sealed in a tungsten crucible. Single crystals were grown from the molten liquid by the Bridgman method using a tungsten heater furnace, which was controlled just above each melting temperature of more than 2000 °C. Single crystals thus grown have a bullet shape with a size of 14 mm (diameter) $\times$ 20 mm (height).

To examine the sample quality in detail, we divided each ingot into three pieces of bottom, middle and upper parts, and measured the electrical resistivity of each piece. We show the temperature dependence of the electrical resistivity of the bottom and upper parts of the CeTe single crystal in Fig. 1. The 4 N Ce was used for sample A. It is noted that residual resistivity ratio (RRR) of the upper part is much larger than that of the bottom part, indicating that the upper part has higher quality. This is also true for the other La mochalcogenides and is contrary to what we expected from previous experience. We expected that the quality of the upper part was worst, because the upper part solidifies last in the present growth process and then impurities usually accumulate in the upper part. It should be pointed out that the overall feature of the electrical resistivity of the upper part is significantly different from that reported previously.[3] For comparison, we also show in Fig. 1 the electrical resistivity of the low-quality CeTe single crystal (sample B) which was grown using the Ce metal with 3 N purity. It had a similar RRR value to that reported previously. Such disagreement between the previous and present reports can be also seen in magnetic properties described later.

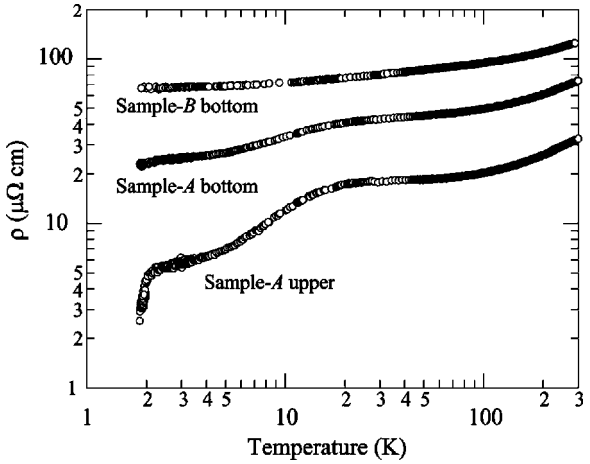

FIG. 1. Temperature dependence of the electrical resistivity of CeTe grown from the stoichiometric molten liquid. "Sample A" and "sample B" were prepared using the Ce metal with 4 and 3 purity, respectively.

We performed another test for CeTe to examine the growth process. The sample was heated again up to 1000 °C just after the single crystal growth process and kept about 1 day. We have found that a small amount of another phase with Th_3P_4 structure, which is probably Ce_3Te_4, is formed in the bottom part, while no trace of such compound was found in the upper part. This observation suggests that the crystal with off-stoichiometric composition segregates from the stoichiometric molten liquid and CeTe is likely to include a large amount of vacancies at the Ce sites. Accordingly, the content of Ce in the molten liquid increases as the crystal grows. The upper part with a stoichiometric composition seems to segregate from the molten liquid with a Ce-rich composition. This behavior is probably also common to the La monochalcogenides. The lattice constants and RRR values of the upper parts are summarized in Table II. The lattice constants of the upper parts are 0.001–0.002 Å larger than those of the bottom parts on an average, probably reflecting the lower concentration of the vacancies in the upper part. Here, it should be noted that the true RRR value of CeTe seems to be larger than that listed in Table II, probably more than 20, because its resistivity continues to decrease even at the lowest temperature of the measurement. We cut small pieces from the upper part for both the magnetization and dHvA effect measurements.

The direct current (dc) magnetization was measured down to 0.5 K by the standard extraction technique using a ^{3}He cryostat in magnetic fields up to 8 T. The dHvA effect mea-

TABLE II. Lattice constant and RRR of high quality LaX_c and CeTe single crystals obtained in this work.

	Lattice constant (Å)	RRR = R(300 K)/R(1.5 K)
LaS	5.852	15
LaSe	6.066	21
LaTe	6.435	20
CeTe	6.369	18

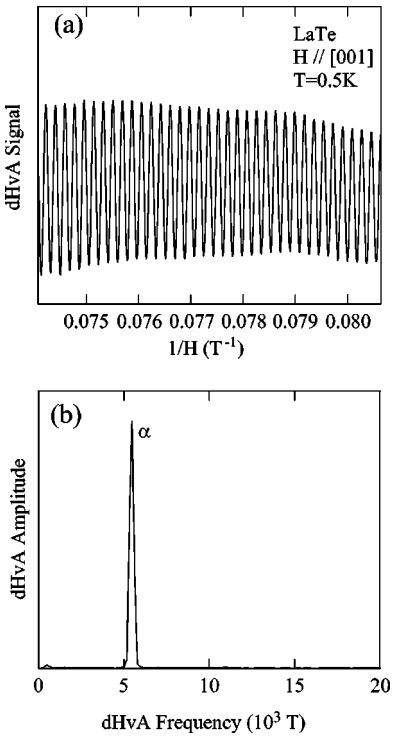

FIG. 2. (a) dHvA oscillation of LaTe at $T=500$ mK and (b) its Fourier spectrum. The magnetic field is applied for the [001] direction.

surements were performed by the conventional field modulation technique using a ^{3}He cryostat inmagnetic fields up to 15 T and a dilution refrigerator in magnetic fields up to 20 T in the temperature range from 20 mK to 1.0 K. The frequency of the modulation field was mostly 67 Hz, while the lower frequency of 17 Hz was used for the measurements of effective masses to decrease the heating effect.

III. RESULT AND DISCUSSION

A. LaX$_c$

We have successfully observed the dHvA signal in all LaX$_c$. Figure 2(a) shows a typical dHvA oscillation of LaTe at $T=500$ mK in the field along the [001] direction. Its Fourier spectrum is shown in Fig. 2(b) where the frequency labeled as α is clearly observed. Figure 3 shows the angular dependences of the dHvA frequencies for LaX$_c$'s. It is clearly seen that their overall features are similar to each other. The dHvA frequency at the same field angle decreases from that of LaS to that of LaSe and then to that of LaTe. The characteristic angular dependence of the dHvA frequency is well reproduced assuming ellipsoidal Fermi surfaces centered at the X points of the Brillouin zone whose major axis is parallel to the Γ-X high symmetry line. They are shown as dotted (LaS), dashed (LaSe), and solid (LaTe) lines in Fig. 3. The dHvA signal has not been observed in LaTe around the [001] and [110] directions. This imply that the ellipsoidal Fermi surfaces are connected at the Γ point and that the conduction band does not cross E_F in the vicinity of the Γ point on the Γ-X high symmetry line. In fact, the ARPES

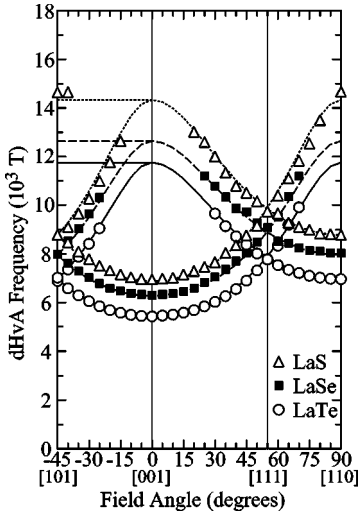

FIG. 3. Angular dependence of the dHvA frequencies for LaX$_c$ (X$_c$=S, Se, Te). Open triangles, closed squares, and open circles are experimental values for LaS, LaSe, and LaTe, respectively. Dotted, dashed, and solid lines show calculated results assuming the ellipsoidal Fermi surfaces centered at the X points of the Brillouin zone.

measurement[10] shows that the conduction band, which is derived from the 5*d* orbit of the La ion, is located just below E_F at the Γ point in LaTe. This missing part of the frequency branch becomes narrower for LaSe. It becomes more narrower for LaS for the [001] direction and the dHvA signal appears at the [110] direction. This means that the ellipsoidal Fermi surfaces in LaSe do not connect with each other at the Γ point. The present observation of the Fermi surfaces is consistent with the band structures observed by the ARPES measurement. However, according to the ARPES measurement, the dHvA signal should be observed around [001] direction in LaS. The reason is not clear at present stage. On the other hand, the two small electron pockets have been observed by the ARPES measurement in LaTe but they have not been detected in this study. In CeTe whose quality seems to be higher than that of LaTe, one small Fermi surface have been detected as described later. Therefore, the missing of the two small Fermi surface is most likely attributed to the worse sample quality of LaTe. The volumes surrounded by the Fermi surfaces of LaX$_c$ are estimated to be very close to 50% of that of the first Brillouin zone. It is noted that the small electron pockets does not significantly contribute to the total volume. Therefore, LaX$_c$'s are uncompensated metals with one conduction electron per formula unit, and the systematic decrease of the dHvA frequency is mainly ascribed to the systematic increase of the lattice constant from that of LaS to that of LaTe.

From the temperature dependence of the amplitude of the dHvA signal, we determined the cyclotron effective masses of LaX$_c$'s. They are summarized in Table III. Every cyclotron effective mass is close to $1m_0$ of the electron rest mass.

B. CeTe

1. Magnetic properties of CeTe

We have measured the dc magnetization ($M_{[hkl]}$) of CeTe under magnetic fields (H) up to 8 T along [*hkl*]=[001], [111], and [110] directions.

TABLE III. Cyclotron effective masses of LaX_c's for the field along the [001], [111], and [110] directions.

	[001]	[111]	[110]
LaS	$0.78m_0$	$1.08m_0$	$0.96m_0$
LaSe	$0.83m_0$	···	$1.02m_0$
LaTe	$0.84m_0$	$1.34m_0$	$1.08m_0$

Figure 4 shows the temperature dependence of M/H for various magnetic fields in the temperature range from 0.5 to 4 K. Let us see the behavior of $M_{[001]}/H$ first. At the low magnetic field of 0.1 T, $M_{[001]}/H$ exhibits a well-defined kink at around 2 K that is a characteristic behavior of the type-II antiferromagnetic order. On the other hand, $M_{[001]}/H$ exhibits a discontinuous change at 0.5 T instead of the kink, suggesting that a ferromagnetic component is induced below 1.8 K. This discontinuous change becomes weaker with increasing magnetic field, and no trace of the discontinuity remains at 8 T. Similar field dependence is also observed in $M_{[110]}/H$-T curves. On the other hand, the kink of $M_{[111]}/H$ is observed up to 3 T, and the ferromagnetic component appears at 4 T, although the $M_{[111]}/H$ change at the transition is rather gradual compared to those for the two other directions. Therefore, the phase above 4 T in the [111] direction certainly has a different character from those above 0.5 T in the [001] and [110] directions.

Figure 5 shows the dc magnetization as a function of the magnetic field along the [001], [111], and [110] directions at 0.5 K. The transition in the [111] direction from the type-II antiferromagnetic phase to the phase with the ferromagnetic component mentioned earlier is clearly seen on the $M_{[111]}-H$ curve at around 3.5 T. Below 3.5 T, $M_{[111]}$ increases linearly with the magnetic field, reflecting the antiferromagnetic state of this phase. On the other hand, the transition to the phase with the ferromagnetic component around 0.1–0.5 T on the $M_{[001]}-H$ and $M_{[110]}-H$ curves could not be detected probably because of too small changes of the magnetization. However, the $M_{[001]}-H$ and $M_{[110]}-H$ curves have convex shapes in contrast to the H-linear shape of the $M_{[111]}-H$ curve below 3.5 T. This fact clearly indicates that

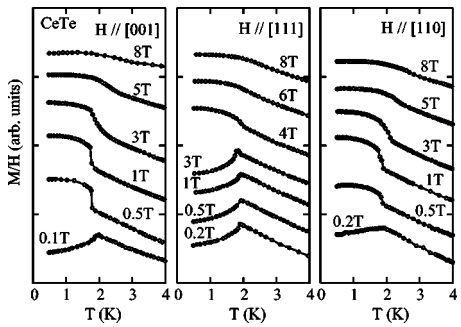

FIG. 4. Temperature dependence of M/H of CeTe for various magnetic fields along [001], [111], and [110] directions. For clarity the M/H curves are displaced vertically.

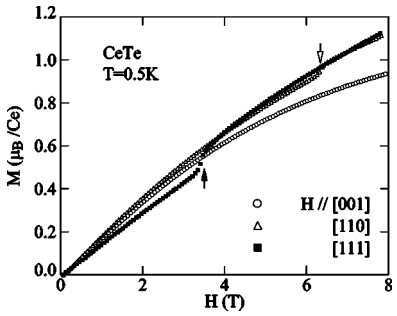

FIG. 5. Magnetization of CeTe as a function of the magnetic field along the [001], [111], and [110] directions at 0.5 K.

the phases above 0.5 T in the [100] and [110] directions are different from the type-II antiferromagnetic state. Above 0.5 T, $M_{[001]}$ doesnot show any discontinuous change up to 8 T, while $M_{[110]}$ exhibits a second transition at around 6.2 T. Here, it should be noted that the magnetization of CeTe exceeds the magnetic moment 0.71 μ_B of the Γ_7 ground state at around 5 T. This means that the magnetic ground state of CeTe under the magnetic field is a mixture of Γ_7 and Γ_8 states arising from the small crystal field splitting. It is also noted that the magnetic properties observed in this study do not agree with those reported previously.[6,4] $M_{[111]}$ reported by Hulliger *et al.* does not show any discontinuous change up to 9 T and $M_{[001]}$ and $M_{[111]}$ show almost the same field dependence below 3 T. On the other hand, Ravot et.al. report a small step at around 2 T associated with a hysteresis on the $M_{[001]}-H$ curve. The difference with those in the previous reports indicates that the magnetic properties of CeTe are very sensitive to the sample quality as well as the transport properties. We suspect that the magnetic phases of CeTe are formed based on a delicate balance among the several exchange interactions because the face-centered-cubic lattice of CeTe is sensitive to the competition of the exchange interactions. Our ARPES measurements[10] suggest that there are two types of the d-f exchange interactions in CeTe, i.e., the on-site d-f ferromagnetic exchange interaction and the intersite d-f antiferromagnetic exchange interaction. The latter arises from the intersite d-f hybridization through the valence p band. Vacancies and impurities presumably destroy the delicate balance between the exchange interactions.

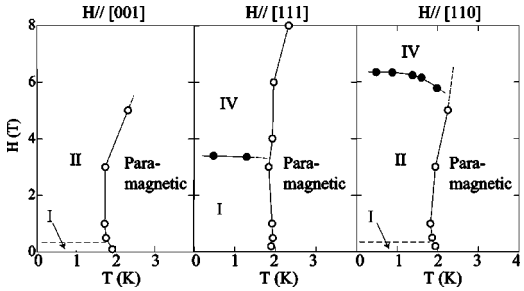

FIG. 6. Magnetic phase diagram of CeTe. Closed and open circles are determined by the M vs H and M/H vs T measurements, respectively.

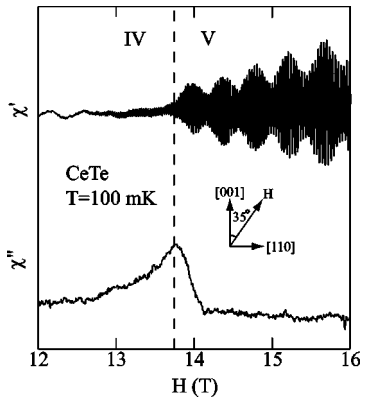

FIG. 7. Field dependence of the ac susceptibility of CeTe at $T=100$ mK. The applied field direction is tilted 35° from [001] toward [110]. χ' and χ'' are real and imaginary parts of the ac susceptibility, respectively.

Summarizing the characteristic changes observed in the temperature dependence of M/H and the field dependence of the magnetization, we propose the magnetic phase diagram for CeTe. Figure 6 shows those in the [001], [111], and [110] directions as a function of the magnetic field and temperature. Phase I is the type-II antiferromagnetic phase. Phase II is characterized by the discontinuous change of the M/H vs T curves. phase IV is characterized by the discontinuous change at around 3.5 T on the M-H curve in the [111] direction. It should be noted that phase IV is not an induced ferromagnetic phase as described later. Nevertheless, the transition temperature between phase IV and the paramagnetic phase increases with increasing magnetic field as well as that between phase II and the paramagnetic phase in the [001] direction does. Such behavior of the phase boundary is quite exceptional for the magnetic transition, while it is rather commonly observed for the quadrapole order transition.[11,12] Although the magnetic ground state of CeTe is the Γ_7 doublet without the orbital degrees of freedom, the Γ_8 quartet excited state certainly mixes into the ground state under the magnetic field as mentioned before. Therefore, the field-induced phases of CeTe are likely to relate to the quadrapole order.

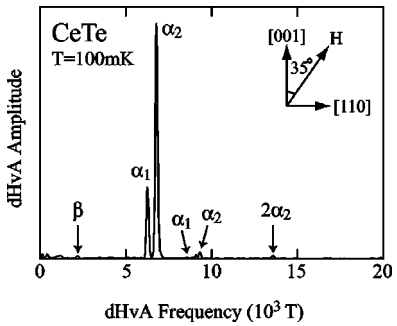

FIG. 9. Fourier spectrum of the dHvA oscillation in phase V of CeTe at $T=100$ mK. The magnetic field direction is tilted 35° from [001] toward [110].

We determined the magnetic phase boundaries also by the dHvA effect measurement. In Fig. 7, we show, as an example, the alternating current (ac) susceptibility as a function of the magnetic field for the direction tilted 35° from [001] toward [110] at $T=100$ mK. The oscillation of the real part is the dHvA signal. At $H=13.8$ T, the real part (χ'') remarkably changes its oscillatory amplitude and wave form. Moreover, the imaginary part (χ'') forms a peak at the same magnetic field. Since theoscillatory amplitude and waveform are related to the Fermi surface properties, their changes suggest that the electronic structure is modified there. The modification is presumably due to a change of the magnetic Brillouin zone caused by the change of the magnetic structure.

By collecting such transition points, we have obtained the magnetic phase diagram of CeTe at $T=100$ mK as a function of the field strength and direction. It is shown in Fig. 8. In addition to the phases described earlier, we have found phases III and V. Therefore, CeTe has at least five magnetic phases at $T=100$ mK. The open circles in the [001] and

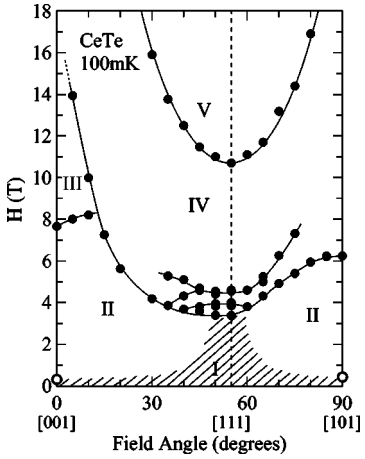

FIG. 8. Magnetic phase diagram of CeTe at $T=100$ mK as a function of the field strength and direction determined by the dHvA effect measurement (closed circles). Open circles are determined by the dc magnetization measurement.

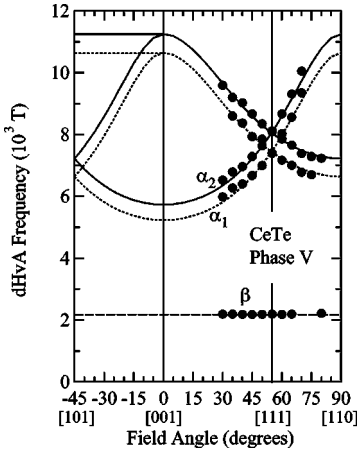

FIG. 10. Angular dependence of the dHvA frequencies in phase V of CeTe. Doted and solid lines for α_1 and α_2 branches show calculated results assuming the ellipsoidal Fermi surfaces centered at the X points of the Brillouin zone.

TABLE IV. Effective masses of the α_1 and α_2 branches determined for two different field ranges in phase V of CeTe. The applied field direction is tilted 35° from [001] toward [110].

Field range	17.6–15.1 T	16.2–14.0 T
α_1	$10.8m_0$	$12.2m_0$
α_2	$5.9m_0$	$6.5m_0$

[101] directions denote the boundaries of phase I determined by the dc magnetization measurements as described earlier. Here, it should be noted that the phase above phase I is not phase II but IV in the vicinity of the [111] direction. The other boundaries of phase I are drawn based on the ac susceptibility measurement but there is an ambiguity in the value of the boundary field due to the gradual change of the ac susceptibility at the transition field. Since phase I is known to be the type-II antiferromagnetic state that has probably the four-***k*** structure, the complicated boundary between phases I and IV in the [111] direction is possibly related to the successive spin flop from the four-***k*** structure. We have succeeded to observe the dHvA effect in phases IV and V.

2. dHvA effect in CeTe

At first, we present the results of the dHvA effect in phase V. As shown in Fig. 7, the oscillatory feature in phase V of CeTe above 13.8 T is distinctly different from that of LaTe, suggesting that several oscillations of different frequencies are superimposed. Figure 9 shows its Fourier spectrum. By considering the angular dependence of the dHvA frequency described later, we can assign three frequencies labeled as α_1, α_2, and β to the three different fundamental frequency. The frequency labeled as $2\alpha_2$ is a second harmonic frequency of α_2.

Figure 10 shows the dHvA frequency of CeTe in phase V as a function of the field angle. We could observe the dHvA signal only in a limited angle range around [111] because necessary magnetic field is too high to enter phase V in other field directions in Fig. 8. As seen in Fig. 10, the frequency of the β branch is very small and its flat shape suggests that it arises from a small spherical Fermi surface. Assuming a spherical shape centered at the Γ point, the Fermi wave vector is estimated to be 0.2 Å^{-1}. The size is in good agreement with that of larger one of the two electron pockets observed in the ARPES measurement.[10] The volume of the Fermi surface of the β branch is less than 1% of the first Brillouin zone as mentioned earlier. On the other hand, the angular dependence of the α_1 branch is very similar to that of the α_2 branch. They are also similar to that of the α branch of LaTe, although we could not determine the branch shape unambiguously because of the limited angle for the observation. Assuming the ellipsoidal Fermi surfaces for these α_1 and α_2 branches as we do for LaTe, each of them is estimated to occupy about 50% volume of the first Brillouin zone. Therefore, it is likely that the α branch in LaTe splits into the α_1 and α_2 branches in phase V of CeTe, probably because the conduction band splits due to the exchange interaction with the $4f$ electrons. Since the Fermi surface has the same shape as that of LaTe or is consistent with that of the paramagnetic phase observed in the ARPES measurement, we believe that phase V is the ferromagnetic state induced by the strong external magnetic field.

From the temperature dependence of the dHvA amplitude, we have determined the effective masses of the α_1 and α_2 branches for two different field ranges in phase V. They are shown in Table IV. The effective masses of both branches are remarkably enhanced compared to that of LaTe and become smaller in the higher field range. The magnetic field dependence may be interpreted in the framework of the competition between the Kondo effect and magnetic field. However, it seems to be beyond this framework that the effective masses of the α_1 and α_2 branches are very much different. Here, we compare the α branch of CeTe with the ζ branch of $CeAl_2$. That is a typical Kondo compound which shows the antiferromagnetic order below 3.85 K.[13] The ζ branch of $CeAl_2$ has a similar size of the Fermi surface as that of the α branch of CeTe and splits into the majority and minority spin bands in the induced ferromagnetic phase above about 6 T. Some characteristic values of them are summarized in Table V. Here, the spin splitting energy ΔE_{ex} are calculated from the following equation:

$$\Delta F = F_2 - F_1 = \frac{m^*}{2m_0\mu_B}\Delta E_{\text{ex}}, \tag{1}$$

where ΔF is the difference of the dHvA frequencies from the majority spin (F_2) and minority spin (F_1) Fermi surfaces, and m^* is an average value of the effective masses of the split branches. From Eq. (1), ΔE_{ex} of the α branch is estimated to be 7 meV, which is similar to $\Delta E_{\text{ex}}=10$ meV of $CeAl_2$, and is much smaller than $E_F=1.62$ eV of CeTe evaluated from the ARPES measurement.[10] Nevertheless, the effective masses of the α_1 and α_2 branches are very much different in contrast to those of the ζ branch of $CeAl_2$. This is a quite exceptional case among Kondo compounds where the effective masses can be very different only when the sizes of up and down Fermi surfaces are very different or the exchange splitting is very large. A similar large difference of the masses has been found in $PrPb_3$ and $CePd_2Si_2$.[14,15] Anoma-

TABLE V. Comparison of $CeAl_2$ ζ branch[13] and CeTe α branch F means dHvA frequency, and suffixes 1 and 2 indicate minority and majority spin bands formed by the spin splitting, respectively. The applied field is parallel to the [111] direction in $CeAl_2$ and tilted 35° fron [001] toward [110] in CeTe.

	F_2(T)	F_1(T)	m_2^*	m_1^*	$\Delta F(=F_2-F_1)$(T)	ΔE_{ex}(meV)
$CeAl_2$ ζ branch	6645	5300	14.7 m_0	14.6 m_0	1350	10
CeTe α branch	6790	6270	$11.5m_0$	$6.1m_0$	520	7

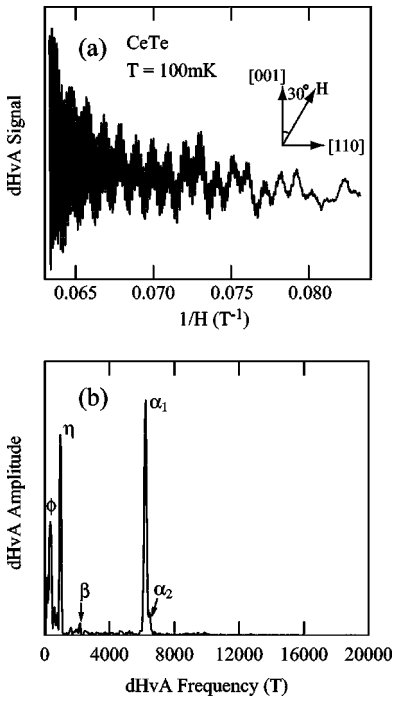

FIG. 11. (a) dHvA oscillation of CeTe in phase IV at $T = 100$ mK and (b) its Fourier spectrum. The magnetic field direction is tilted 30° from [001] to [110].

lous spin dependence of the dHvA signal has been also reported in CeB_6 and $Ce_{1-x}La_xB_6$ where the signal arises only from either up or down spin electrons.[16] Understanding of these strongly spin dependent effects seems to be a crucial issue of the strongly correlated electron systems.

Finally, we present the results of the dHvA effect measurement in phase IV. Figure 11(a) shows a typical dHvA oscillation in phase IV at $T = 100$ mK. The field direction is tilted 30° from the [001] direction toward the [110] direction. The oscillatory feature in phase IV of CeTe is obviously different from that in phase V of CeTe and also from that of LaTe, suggesting that the Fermi surfaces are different in phase IV. Figure 11(b) shows its Fourier spectrum. Five fundamental frequencies labeled as α_1, α_2, β, η, and ϕ are found. Figure 12 shows the dHvA frequency in phase IV of CeTe as a function of the field angle. In addition to the branches in Fig. 11(b), two branches labeled as γ_1 and γ_2 are found. The angular dependences of the α_1 and α_2 branches in phase IV are very similar to those of the α_1 and α_2 branches in phase V and also that of the α branch of LaTe. This fact suggests that the main Fermi surface in phase IV has an ellipsoidal shape and is centered at the X point of the Brillouin zone. It also indicates that the conduction band splits into the majority and minority spin bands due to the exchange interaction between the conduction and $4f$ electrons similarly to the case of phase V. It is also noted that the spin splitting ΔF is smaller than that of phase V. On the other hand, the γ_1, γ_2, η, and ϕ branches are not observed both in phase V of CeTe and in LaTe. Furthermore, it should be noted that the η and ϕ branches have fine structure and that the γ_1, γ_2 branches are not observed in the ARPES measurement of CeTe in the paramagnetic phase.

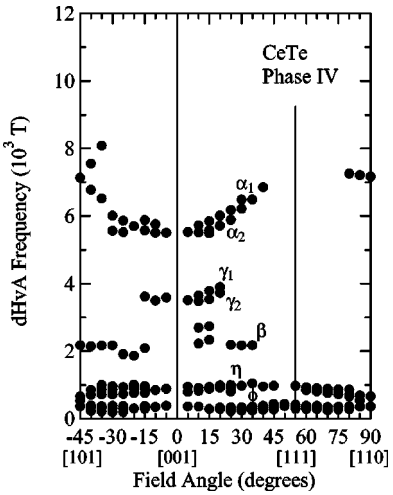

FIG. 12. Angular dependence of the dHvA frequencies in phase IV of CeTe.

The smaller ΔF in phase IV probably indicates that the exchange energy ΔE_{ex} in phase IV is smaller than that in phase V, suggesting a smaller ferromagnetic component in phase IV. Therefore, phase IV is considered to be an antiferromagnetically ordered state with a ferromagnetic component. This antiferromagnetic order forms a magnetic Brillouin zone to generate new branches in phase IV.

IV. CONCLUSION

High quality single crystals of LaX_c's with $X_c = S$, Se, Te, and CeTe have been grown. We have measured the de Haas-van Alphen effect of these compounds and the magnetic properties of CeTe. The Fermi surfaces of LaX_c's have nearly ellipsoidal shapes centered at the X points of the Brillouin zone. The cyclotron effective masses have been determined to be $1m_0$. On the other hand, CeTe has a rather complicated magnetic phase diagram which is very different from that predicted by the previous works. We have succeeded to observe the dHvA effect in phases V and IV, which are probably an induced ferromagnetic state and an antiferromagnetic state with a ferromagnetic component, respectively. The main Fermi surface of CeTe in phases V and IV splits into those of the majority and minority spin bands due to the exchange interaction between the $4f$ and conduction electrons, and both of them have very similar shape to that of LaTe. Strongly enhanced cyclotron effective masses have been observed in phase V. However, the mass enhancement factor of the minority spin surface considerably differs with that of the majority spin surface.

ACKNOWLEDGMENTS

The authors would like to thank M. Kikuchi and M. Suzuki for their technical support. This work was partially supported by a Grant-in-Aid for Scientific Research from the Minister of Education, Culture, Sports, Science and Technology.

*Electronic address: aochiai@mail.clts.tohoku.ac.jp

[1] M. Ohashi, D. Kindo, N. Sato, T. Suzuki, T. Komatsubara, H. Takahashi, and N. Mori, Rev. High Pressure Sci. Technol. **7**, 611 (1998).
[2] P. Haen, F. Lapierre, J. M. Mignot, R. Tournier, and F. Holtzberg, Phys. Rev. Lett. **43**, 304 (1979).
[3] J. Shoenes and F. Hulliger, J. Magn. Magn. Mater. **63&64**, 43 (1987).
[4] D. Ravot, P. Burlet, J. Rossat-Mignod, and L. Tholence, J. Phys. (France) **41**, 1117 (1980).
[5] A. Dönni, A. Furrer, P. Fisher, and F. Hulliger, Physica B **186–188**, 541 (1993).
[6] F. Hulliger, B. Natterer, and H. R. Ott, J. Magn. Magn. Mater. **8**, 87 (1978).
[7] H. R. Ott, J. K. Kjems, and F. Hulliger, Phys. Rev. Lett. **42**, 1378 (1979).
[8] A. Dönni, A. Fuller, P. Fisher, S. M. Hayden, F. Hulliger, and T. Suzuki, J. Phys.: Condens. Matter **5**, 1119 (1993).
[9] H. Matsui, T. Goto, A. Tamaki, T. Fujimura, T. Suzuki, and T. Kasuya, J. Magn. Magn. Mater. **76&77**, 321 (1988).
[10] M. Nakayama, H. Aoki, A. Ochiai, T. Ito, H. Kumigashira T. Takahashi, and H Harima, Phys. Rev. B **69**, 155116 (2004).
[11] J. M. Effantin, J. Rossatmignod, P. Burlet, H. Bartholin, S. Kunii, and T. Kasuya, J. Magn. Magn. Mater. **47&48**, 145 (1985).
[12] T. Tayama, T. Sakakibara, K. Kitanai, M. Yokoyama, K. Tenya, H. Amitsuka, D. Aoki, Y. Ōnuki, and Z. Kletowski, J. Phys. Soc. Jpn. **70**, 248 (2003).
[13] P. H. P. Reinders and M. Springford, J. Magn. Magn. Mater. **79**, 295 (1989).
[14] M. Endo, N. Kimura, A. Ochiai, H. Aoki, T. Terashima, C. Terakura, S. Uji, and T. Matsumoto, Acta Phys. Pol. B **34**, 1031 (2003).
[15] I. Sheikin, A. Gröger, S. Raymond, D. Jaccard, D. Aoki, H. Harima, and J. Flouquet, Phys. Rev. B **67**, 094420 (2003).
[16] N. Harrison, P. Meeson, P.-A. Probst, and M. Springford, J. Phys.: Condens. Matter **5**, 7453 (1993).